Negative refraction and reflection of Gaussian beam on two-dimensional photonic crystal slab

Yuntuan Fang (方云团)[1], Yuzhen Liu (刘玉真)[2], and Tinggen Shen (沈廷根)[3]

[1]*Department of Physics, Zhenjiang Watercraft College, Zhenjiang 212003*

[2]*Department of Physics, Nanjing University of Science and Technology, Nanjing 210094*

[3]*Department of Physics, Jiangsu University, Zhenjiang 212003*

Received July 18, 2005

The refraction and reflection of Gaussian beam on two-dimensional photonic crystal (2DPC) slab are studied by the finite-difference time-domain (FDTD) method. It is shown that 2DPC slab enables negative refraction, which is demystified by the distribution of Poynting vector directions and values inside the 2DPC. A negative Goos-Hänchen shift is also found in the simulation.

OCIS codes: 160.4670, 350.5500, 120.4700, 120.5710.

Negative refraction of electromagnetic waves in "left-handed materials" has become of interest recently because it is the foundation for variety of novel phenomena[1−5]. In particular, it has been suggested that negative refraction leads to super-prism and super-lensing effects[2,6]. These phenomena have been described in the context of an effective-medium theory with negative index of refraction, and at the moment only appear possible in the microwave regime. To explore the possibility of negative refraction in the optical regime, one may turn to photonic crystals (PCs) as interesting alternatives. Recent experimental[7] and theoretical[1] works indicate that negative refraction phenomena in PCs are possible in regimes of negative group velocity and negative effective index above the first band near the Brillouin-zone center. For most simulation works about light wave propagation in PC by finite-difference time-domain (FDTD) method, the results are usually given by only the distribution of electric field for transverse magnetic (TM) polarization[5,8] or magnetic field for transverse electric (TE) polarization[9] in the two-dimensional (2D) plane. In our view, the results obtained by the above methods are not all-around. As have been known, the directions of reflection and refraction should be determined by the direction of Poynting vector $\vec{S} = \vec{E} \times \vec{H}$, i.e., the light line propagation directions, and cannot be indicated by only the electric field or magnetic field distribution. Furthermore, the direction of negative refraction inside PC should be that of group velocity, i.e., energy flow, not of phase velocity. Therefore, in order to obtain exactly the behavior of the reflection and refraction of light on the two-dimensional PC (2DPC), one must give not only the distribution of the values of Poynting vectors but also that of the directions of Poynting vectors. Basing on the above consideration, we carry out simulations that a Gaussian beam interacts with 2DPC slab and observe the behavior of the reflection and refraction of light on the 2DPC.

Numerical simulation is performed based on the FDTD method which is a very powerful method to analyze electromagnetic problem due to its simplicity and accuracy. In a 2D case, the electromagnetic fields can be decoupled into two transversely polarized modes, namely, the TE and the TM modes. For a linear isotropic material in a source-free region, the time-dependent Maxwell's equations can be discretized in space and time by a so-called Yee-cell technique[10]. The following FDTD time stepping formulas are the spatial and time discretizations of Maxwell's equations on a discrete 2D mesh within the x-y coordinate system for the TM mode[10]

$$H_x|_{i,j+\frac{1}{2}}^{n+\frac{1}{2}} = H_x|_{i,j+\frac{1}{2}}^{n-\frac{1}{2}} - \frac{\Delta t}{\mu_0} \frac{E_z|_{i,j+1}^{n} - E_z|_{i,j}^{n}}{\Delta y}, \quad (1)$$

$$H_y|_{i+\frac{1}{2},j}^{n+\frac{1}{2}} = H_y|_{i+\frac{1}{2},j}^{n-\frac{1}{2}} + \frac{\Delta t}{\mu_0} \frac{E_z|_{i+1,j}^{n} - E_z|_{i,j}^{n}}{\Delta x}, \quad (2)$$

where n denotes the discrete time step, i and j denote the discretized grid point in the x-y plane, respectively, Δt is the time increment, and Δx and Δy are the cells between two neighboring grid points along the x and y directions, respectively. The electromagnetic field inside the computation region is modelled by repeatedly applying Eqs. (1) and (2); at each repetition, the whole field distribution is evaluated using the known distribution at the previous step. In our computation, we set 524×484 cells and $\Delta t = \frac{1}{2c\sqrt{(\Delta x)^{-2}+(\Delta y)^{-2}}}$ which can give a stable and convergent solution of the above equations. Similar equations for the TE mode can be easily obtained. Special consideration should be given at the boundary of the finite computational domain, where the fields are updated using special boundary conditions as information out of the domain is not available. Here, we use the perfectly matched layer (PML) method[11] for the boundary treatment.

The present 2DPC is a triangular lattice of air holes in a dielectric material with dielectric constant $\varepsilon = 12.96$, lattice constant $a = 20$ cells and hole radius $r = 0.4a$. The surface normal is along the ΓM direction. Only the TM mode is considered here. The configuration of the 2DPC slab is indicated in Fig. 1. To visualize and analyze light propagation in PC, an equal frequency surface (EFS)[1] in k space of the photonic bands is then introduced, where gradient vectors give the group velocities of the photonic modes. For the current PC, we obtain photonic band structures using the standard plane expansion

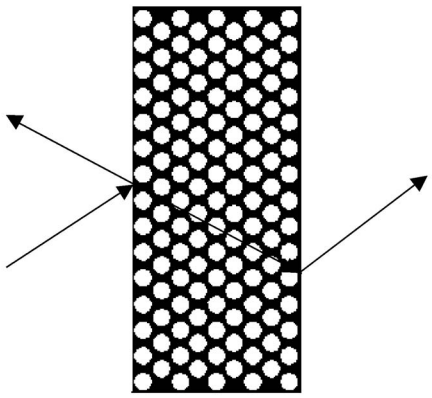

Fig. 1. Configuration of the 2DPC slab and the possible paths of light propagation with negative refraction.

method[12]. For a single mode and E and H polarized waves, the full-vector wave equation of the electromagnetic field $\vec{E}_{(r)}$ and $\vec{H}_{(r)}$ may be obtained from Maxwell's equations and expressed as

$$\frac{\partial}{\partial x}\left[\frac{1}{\varepsilon(r)}\frac{H_k(r)}{\partial x}\right]+\frac{\partial}{\partial y}\left[\frac{1}{\varepsilon(r)}\frac{H_k(r)}{\partial y}\right]+\frac{\omega^2}{c^2}H_k(r)=0, \tag{3}$$

$$\frac{1}{\varepsilon(r)}\left[\frac{\partial^2}{\partial x^2}+\frac{\partial^2}{\partial y^2}\right]E_k(r)+\frac{\omega^2}{c^2}E_k(r)=0, \tag{4}$$

where the subscription k represents the wave propagation vector of the mode, $\varepsilon(r)$ is the position-dependent dielectric constant of the periodic structure, and c is light velocity. Taking advantage of the periodic nature of the problem, the H-field and E-field may be expanded into a sum of plane waves using Bloch's theorem as

$$H_k(r)=\sum_G H_{k+G}\mathrm{e}^{i(k+G)\cdot r}, \tag{5}$$

$$E_k(r)=\sum_G E_{k+G}\mathrm{e}^{i(k+G)\cdot r}, \tag{6}$$

where G represents a lattice vector in reciprocal space, describing the periodic structure. The dielectric constant may be expressed as a Fourier series expansion

$$\frac{1}{\varepsilon(r)}=\sum_G \varepsilon^{-1}(G)\mathrm{e}^{iG\cdot r}, \tag{7}$$

where

$$\varepsilon^{-1}(G)=\frac{1}{A_\mathrm{u}}\int\frac{1}{\varepsilon(r)}\mathrm{e}^{-iG\cdot r}\mathrm{d}r, \tag{8}$$

A_u indicates the area of a unit cell, i.e., the smallest region, that may be used to represent the periodic structure. Finally, by substituting Eqs. (5), (6), and (7) into Eqs. (3) and (4), we find

$$\sum_G (k+G)\cdot(k+G')\varepsilon^{-1}(G-G')H_{k+G}=\frac{\omega^2}{c^2}H_{k+G}, \tag{9}$$

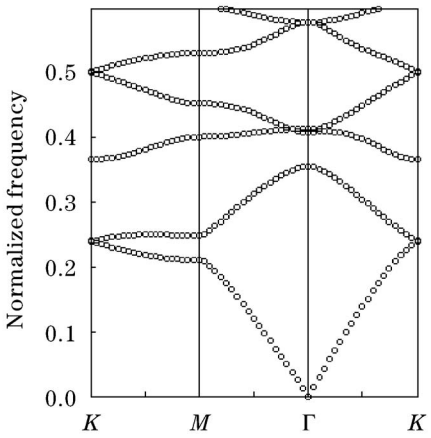

Fig. 2. Calculated photonic band structure.

$$\sum_G |k+G|\,\varepsilon^{-1}(G-G)\,|k+G'|\,E_{k+G}=\frac{\omega^2}{c^2}E_{k+G}. \tag{10}$$

Then a matrix eigenvalue problem is obtained, where, for a fixed wave vector, k, the frequencies ω of the allowed modes in the periodic structure are found as eigenvalues. Basing on the above method, we obtain the photonic band structures for wave vectors along the edges of the irreducible Brillouin zone (BZ) defined by the points Γ, M, and K for the 2DPC, as shown in Fig. 2. The equal frequency contour obtained by crossing the second band with the EFS for normalized frequency $\omega = 0.3(2\pi c/a)$ is circular. For simplicity, the unit of $2\pi c/a$ is omitted later. The propagation of the waves is therefore isotropic, and one can define an isotropic effective refraction index n_eff from the radius of the EFS using Snell's law, which is used to describe the light refraction in PC. For current frequency $\omega = 0.3$, the effective refractive index of the PC is -1.

To observe the behavior of negative refraction, an oblique incident Gaussian beam is incident at an incident angle of $\pi/4$ onto the above 2DPC slab. The source of Gaussian beam is limited at a line and given by the expression $f(x,y,t) = \sin(\omega t)\exp\{-[(x-x_0)^2+(y-y_0)^2]/w^2\}$ with $\omega = 0.3$ and $w = 5a$, where (x_0, y_0) is the center of source, i.e., the position for maximum value of light intensity. The whole conceptual configuration of simulation is shown in Fig. 3(a), in which A (107, 112) is the center of source, two dotted lines refer to 2DPC slab interfaces, the dashed arrow denotes the direction of beam propagation and the peak value position should intersect with the front interface at B (240, 245), the solid arrow refers to the direction of reflection beam according the reflection law. The simulation result is shown in Fig. 3(b), which gives the intensity image of the average Poynting vectors from the calculation space. From Fig. 3(b), we can easily observe the reflective and refractive beam. The negative refraction behavior is clear and consistent with Fig. 1. In order to verify the negative refraction occurring, we further calculate the unit vectors of Poynting vectors in the simulation space, which gives the distribution of the directions of Poynting vectors. As discussed above, they can depict light propagation more exactly. The calculation result is shown in Fig. 4, in which the arrows are the units of Poynting

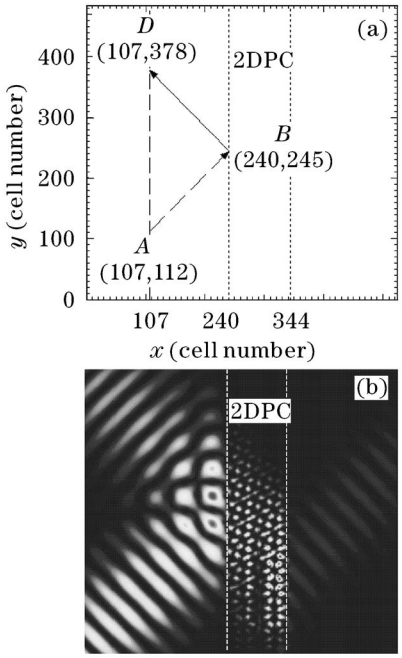

Fig. 3. (a) The whole conceptual configuration of simulation. (b) The intensity image of the average Poynting vectors from the calculation space.

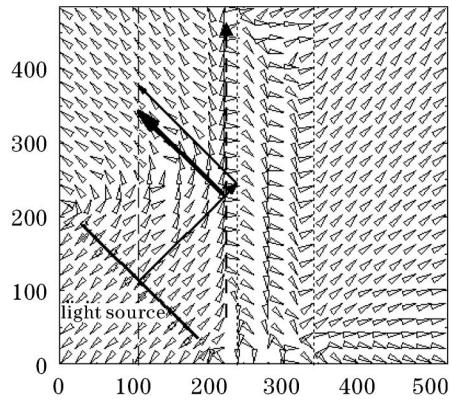

Fig. 4. Distribution of average Poynting vectors in the simulation space.

vectors and indicate the directions of Poynting vectors. Obviously the whole region of Fig. 4 can be separated into incident and reflective parts, the 2DPC slab, and the transmission part. In the incident part and reflective part, the Poynting vectors point to and leave from the 2DPC slab, respectively. Both the directions of the incident and reflective Poynting vectors follow the reflection law. The part of the 2DPC slab is indicated by two dashed lines. The transmission part is behind the 2DPC slab. Near the two interfaces of the 2DPC slab, the directions of Poynting vectors change following the negative refraction rule.

On the other hand, a negative Goos-Hänchen shift has been found at an interface between right-handed and left-handed media when total internal reflection occurs[13−15], while a positive Goos-Hänchen shift should occur at an interface between two right-handed media under the same condition, because the energy flow directions near the interface are reverse for the two cases.

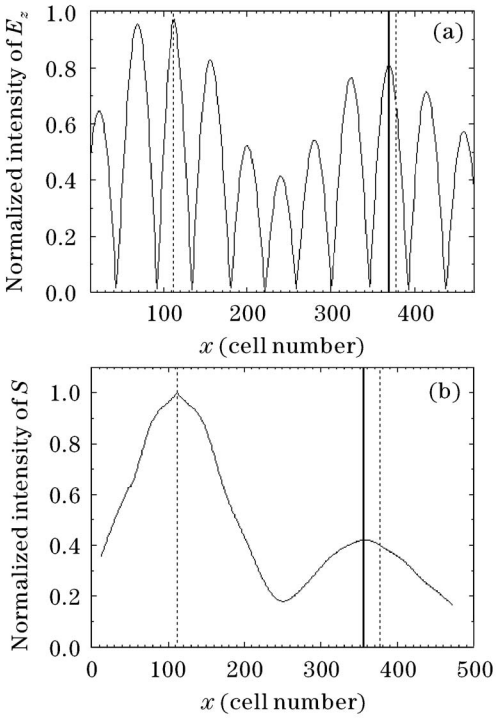

Fig. 5. Values of the electric field (E_z) (a) and the average Poynting vectors (S) (b) along the dashed line in Fig. 3(a).

Since negative refraction also occurs on 2DPC slab, we should think that whether Goos-Hänchen shift occurs at the interface of 2DPC slab. In order to study this question, we draw a line through point A and parallel to the interface, as depicted by the dashed line in Fig. 3(a). If there is no shift for the reflective wave, the reflective beam is indicated by the solid arrow. If so, we should measure a maximum value of reflective light intensity at D (107, 378). Then we calculate the value of the electric field (E_z) and the average Poynting vectors (S) along the dashed line, respectively. As a result, the maximum values of E_z and S in the dashed line are at (107, 368) and (107, 356), both not at D (107, 378), as shown in Fig. 5. In the figure, the positions of the incident beam peak and the speculating reflection beam peak are indicated by the vertical dotted lines, the positions of reflective beam peaks obtained in our simulation are indicated by the vertical solid lines. In both cases, a negative Goos-Hänchen shift has been found, but the shift values are different, because the electric field is an instantaneous value. According to Fig. 5(b), the negative Goos-Hänchen shift is about 22 cells, i.e., $1.1a$. In addition, we should notice that the negative Goos-Hänchen shift for the 2DPC slab does not need the condition of total internal reflection because of the following machanism. In Fig. 4, there is a thin layer of Poynting vectors near the left interface and parallel to the interface, indicated by a long dashed arrow. This layer of Poynting vectors indicates some surface modes that occur near the PC interface under the condition of negative refraction of 2DPC[16]. Because of the existence of the surface wave, the reflection occurs at a surface in front of the interface, not just at the interface, as indicated by the wide arrow in Fig. 4. Then the negative Goos-Hänchen shift occurs.

In conclusion, the distributions of average Poynting

vectors in the 2DPC slab verify the negative refraction phenomena. Under the condition of negative refraction, a negative Goos-Hänchen shift also occurs at the interface of the 2DPC slab.

This work was supported by the Natural Science Foundation of Jiangsu Province of China under Grant No. BK2004059. Y. Fang's e-mail address is fang_yt1965@sina.com.

References

1. M. Notomi, Phys. Rev. B **62,** 10696 (2000).
2. J. B. Pendry, Phys. Rev. Lett. **85,** 3966 (2000).
3. M. Cubukcu, K. Aydin, E. Ozbay, S. Foteinopoulou, and C. M. Soukoulis, Nature **423,** 604 (2003).
4. P. V. Parimi, W. T. Lu, P. Vodo, and S. Sridhar, Nature **426,** 404 (2003).
5. C. Luo, S. G. Johnson, J. D. Joannopoulos, and J. B. Pendry, Phys. Rev. B **65,** 201104 (2002).
6. P. Kolinko and D. R. Smith, Opt. Express **11,** 640 (2003).
7. H. Kosaka, T. Kawashima, A. Tomita, M. Notomi, T. Tamamura, T. Sato, and S. Kawakami, Phys. Rev. B **58,** R10096 (1998).
8. C. Luo, S. G. Johnson, J. D. Joannopoulos, and J. B. Pendry, Opt. Express **11,** 746 (2003).
9. X. Wang, Z. F. Ren, and K. Kempa, Opt. Express **12,** 2919 (2004).
10. M. Qiu and S. He, Phy. Rev. B **61,** 12872 (2000).
11. Y. Fang and T. Shen, Chin. Opt. Lett. **3,** 261 (2005).
12. Y. Fang, Laser Phys. Lett. **1,** 383 (2004).
13. P. R. Berman, Phy. Rev. E **66,** 067603 (2002).
14. I. V. Shadrivov, A. A. Zharov, and Y. S. Kivshar, Appl. Phys. Lett. **83,** 2713 (2003).
15. R. W. Ziolkowski, Opt. Express **11,** 662 (2003).
16. X. Wang and K. Kempa, Phys. Rev. B **71,** 233101 (2005).